Supporting Information

Predictive Design of Ordered Mesoporous Silica with Well-Defined, Ultra-Large Mesopores

Charlotte Vogler[1], Stefan Naumann[1], Johanna R. Bruckner[2,]*

[1] University of Stuttgart, Institute of Polymer Chemistry,
Pfaffenwaldring 55, 70569 Stuttgart, Germany.

[2] University of Stuttgart, Institute of Physical Chemistry,
Pfaffenwaldring 55, 70569 Stuttgart, Germany.
johanna.bruckner@ipc.uni-stuttgart.de

Content

1 Synthesis of triblock copolyethers

1.1 Catalyst synthesis

The **NHO 1** (*N*-heterocyclic olefin) was prepared according to a published procedure,[1,2] a schematic synthetic route is provided in Figure S1.

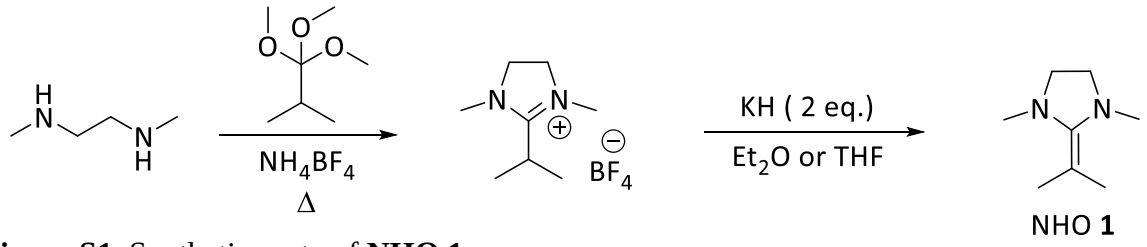

Figure S1. Synthetic route of **NHO 1**.

1.2 Polymerization

Each polyether was analyzed via ^{1}H NMR (nuclear magnetic resonance) to determine the average PPO (polypropylene oxide) block length (*n*/2). For one representative example, the ^{1}H NMR is depicted in Figure S2 and the relevant polymer signals are denoted.

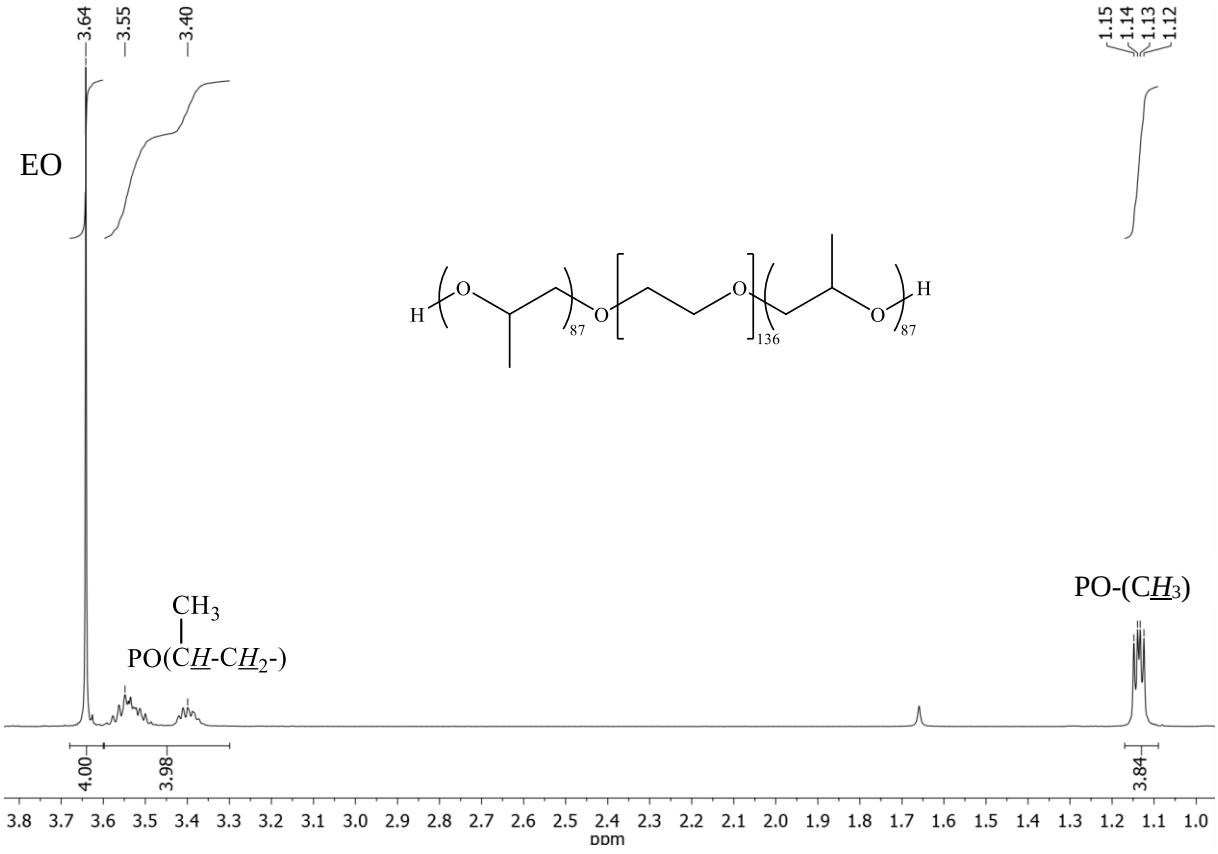

Figure S2. ^{1}H NMR analysis ($CDCl_3$, 400 MHz, 300 K) of a "Reverse Poloxamer" prepared by the action of **NHO 1** and Et_3B.

1.3 Calculation of the hydrophilic to lipophilic balance (HLB)

$$HLB = 20 \cdot \frac{M_{\mathrm{H}}}{M_{\mathrm{PM}}} \qquad \text{Eq. S1}$$

HLB = hydrophilic to lipophilic balance

M_{H} = molar mass of hydrophilic part of the polymer (*here:* PEO (polyethylene oxide))

M_{PM} = total molar mass of the polymer

1.4 Calculation of the dispersity $Đ_{\mathrm{M}}$

$$Đ_{\mathrm{M}} = \frac{M_{\mathrm{w}}}{M_{\mathrm{n}}} \qquad \text{Eq. S2}$$

$Đ_{\mathrm{M}}$ = dispersity[3]

M_{w} = weight-average molar mass

M_{n} = number-average molar mass

All values were determined by gel permeation chromatography (GPC). The dispersity of all block copolymers synthesized is listed in Table S1.

2 Screening for lyotropic liquid crystalline phases

For each polyether, diluted surfactant solutions were prepared with mass fractions in the range of 0 to 100 wt% (10 wt% steps) by weighing the respective amount of the polyether into caps-tubes and further diluting them with the adequate mass of demineralized, double distilled water. Therefore, a Mettler Toledo XP 105 balance was used to ensure an accuracy of 0.1 mg. The water was mixed with the Polyether using the motor handpiece MHX/E from Xenox until homogeneity was reached. Finally, the generated dilution fractions were investigated using different characterization methods.

2.1 Polarized optical microscopy (POM)

For characterization of the lyotropic liquid crystal (LLC) samples, we used an optical microscope DMP 2700 P from Leica, equipped with a Leica DMC2900 camera and the software Leica Application Suite Version 4.4.0. All samples were investigated at room temperature. Samples for polarized optical microscopy were prepared by sucking in the LLC samples into glass tubes from VitroCom by the help of a water jet pump, which were then fused using a methane oxygen burner. Samples of high viscosity were brought on a slide and covered with a cover glass, which was then sealed up with an UV glue.

As shown in Figure S3, typical textures of the a) cubic I_1, b) hexagonal H_α and c) lamellar L_α phase were identified at specific mass fractions. The sample with $w(PPO_{80}\text{-}PEO_{181}\text{-}PPO_{80})$ = 40 wt% is isotropic between crossed polarizers, as typical for cubic phases, in contrast for $w(PPO_{80}\text{-}PEO_{181}\text{-}PPO_{80})$ = 60 wt% and 70 wt%, birefringence is clearly visible, which indicates a hexagonal or lamellar phase.

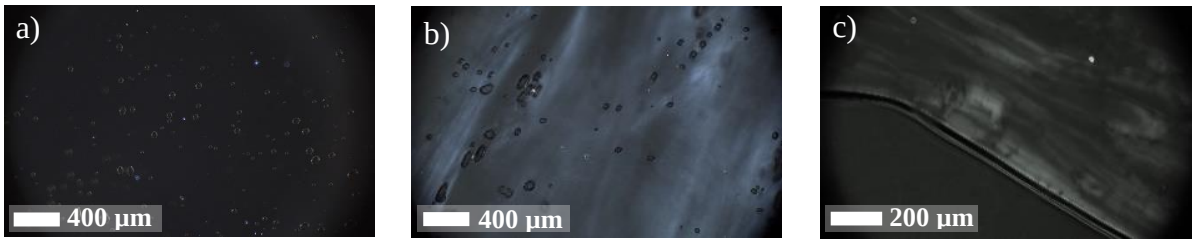

Figure S3. Typical textures of the a) cubic I_1 ($w(PPO_{80}\text{-}PEO_{181}\text{-}PPO_{80}$ = 40 wt%), b) hexagonal H_α ($w(PPO_{80}\text{-}PEO_{181}\text{-}PPO_{80}$ = 60 wt%), and c) lamellar L_α ($w(PPO_{80}\text{-}PEO_{181}\text{-}PPO_{80}$ = 70 wt%), phase. Note that the hexagonal and the cubic phase contains many trapped air bubbles due to high viscosities of the two LLC phases.

2.2 Small-angle X-ray scattering (SAXS)

We confirmed the structures of the LLC phases additionally by SAXS analysis. In all cases, the structure can clearly be assigned by the help of their characteristic pattern, which are shown in Figure S4 for one representative polyether example.

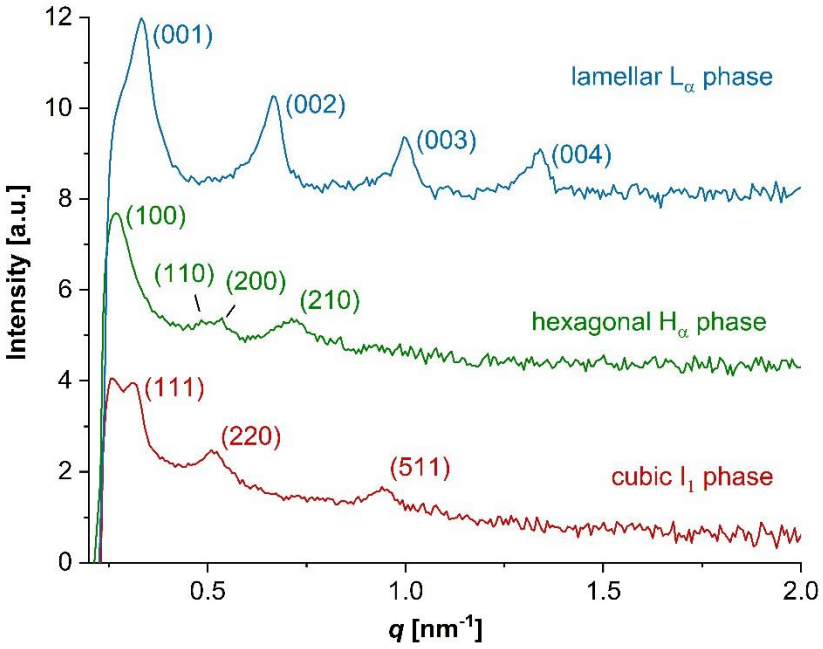

Figure S4. SAXS patterns of three occurring LLC phases formed by PPO_{80}-PEO_{181}-PPO_{80} at w = 40 wt% (face centered cubic I_1 phase), w = 60 wt% (hexagonal H_α phase) and w = 70 wt% (lamellar L_α phase). The Miller Indices (*hkl*) are assigned to the characteristic peaks. The apparent peak at 0.26 nm^{-1}, which occurs in the diffractogram of the I_1 phase, is actually scattering caused by the form factor of the mesopores.

2.3 Differential Scanning calorimetry (DSC)

We checked the stability of the LLC phases for some representative examples from 0 to 100 °C by DSC. No phase transition in the temperature range which is relevant for the templating process (25 to 80 °C), could be observed for the mixtures which were later on used as templates (w = 50-70 wt% for PPO_{80}-PEO_{181}-PPO_{80}).

For sample preparation around 3 mg of each LLC sample was filled in an aluminium pan (PerkinElmer, part number B0169321). For each sample, three measurement cycles were performed with a speed of 5 °C min^{-1} by using a DSC 8000 from PerkinElmer. For analysis only the second heating cycle was used.

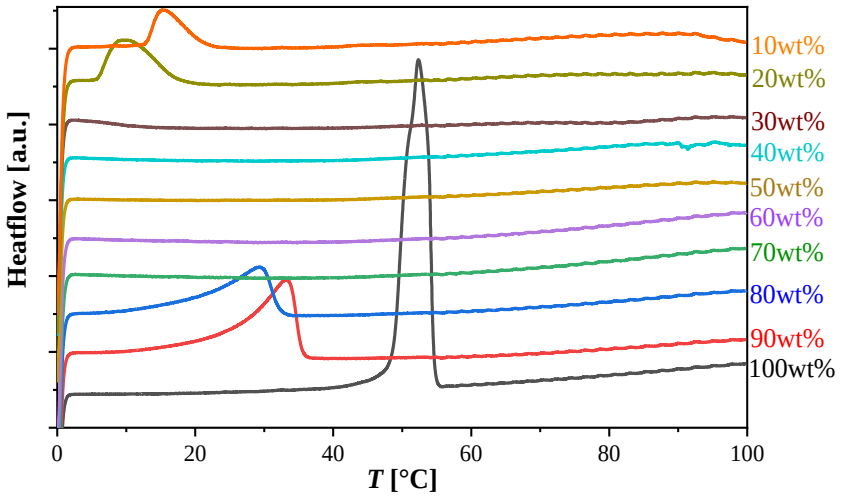

Figure S5. Heat flow while heating of the representative polyether PPO_{80}-PEO_{181}-PPO_{80} with water at different molar ratios.

2.4 Phase diagram

By combination of all results from POM, SAXS and DSC, we generated the phase diagram of one representative polyether (PPO_{80}-PEO_{181}-PPO_{80}), as pictured in Figure S6.

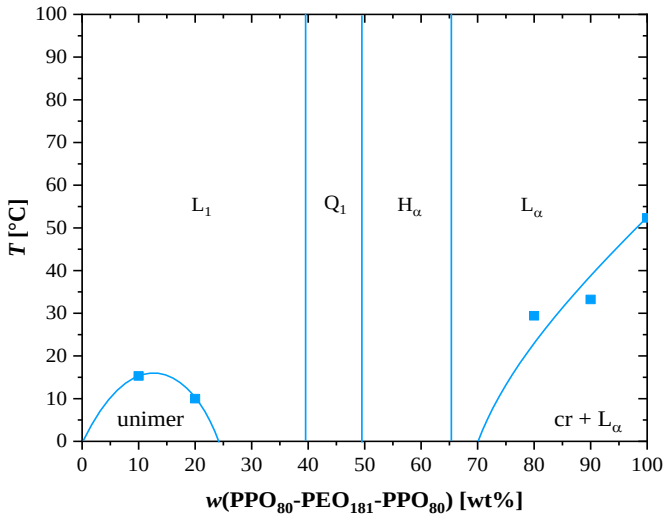

Figure S6. Phase diagram of the PPO_{80}-PEO_{181}-PPO_{80}/water system: L_1 = micellar solution, Q_1 = cubic phase, H_α = hexagonal phase, L_α = lamellar phase, unimer = istropic solution of unimers, cr = crystalline. Samples were investigated at intervals of 10 wt%. Two-phase regions between LLC phases were not investigated in detail and thus were omitted.

3 True liquid crystal templating

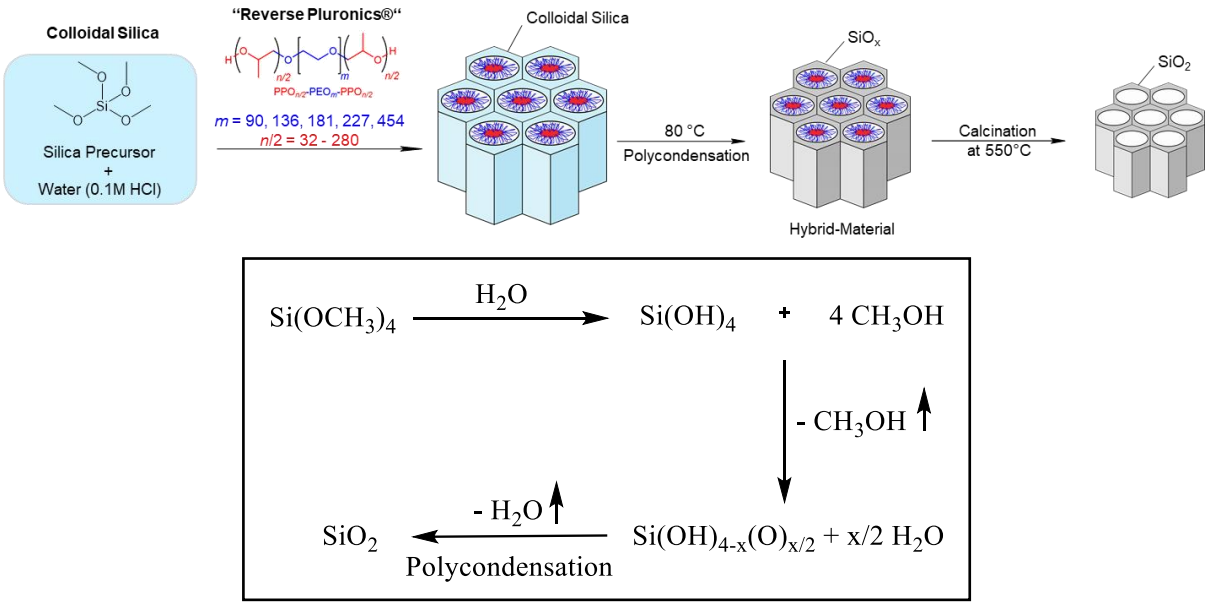

Figure S7. Simplified scheme of the "TLCT" (true liquid crystal templating) process and the detailed polycondensation process to colloidal silica ($Si(OH)_{4-x}(O)_{x/2}$ + *x*/2 H_2O) and fully condensed silica (SiO_2).

4 Characterization of the ordered mesoporous silica materials

4.1 Scanning electron microscopy (SEM)

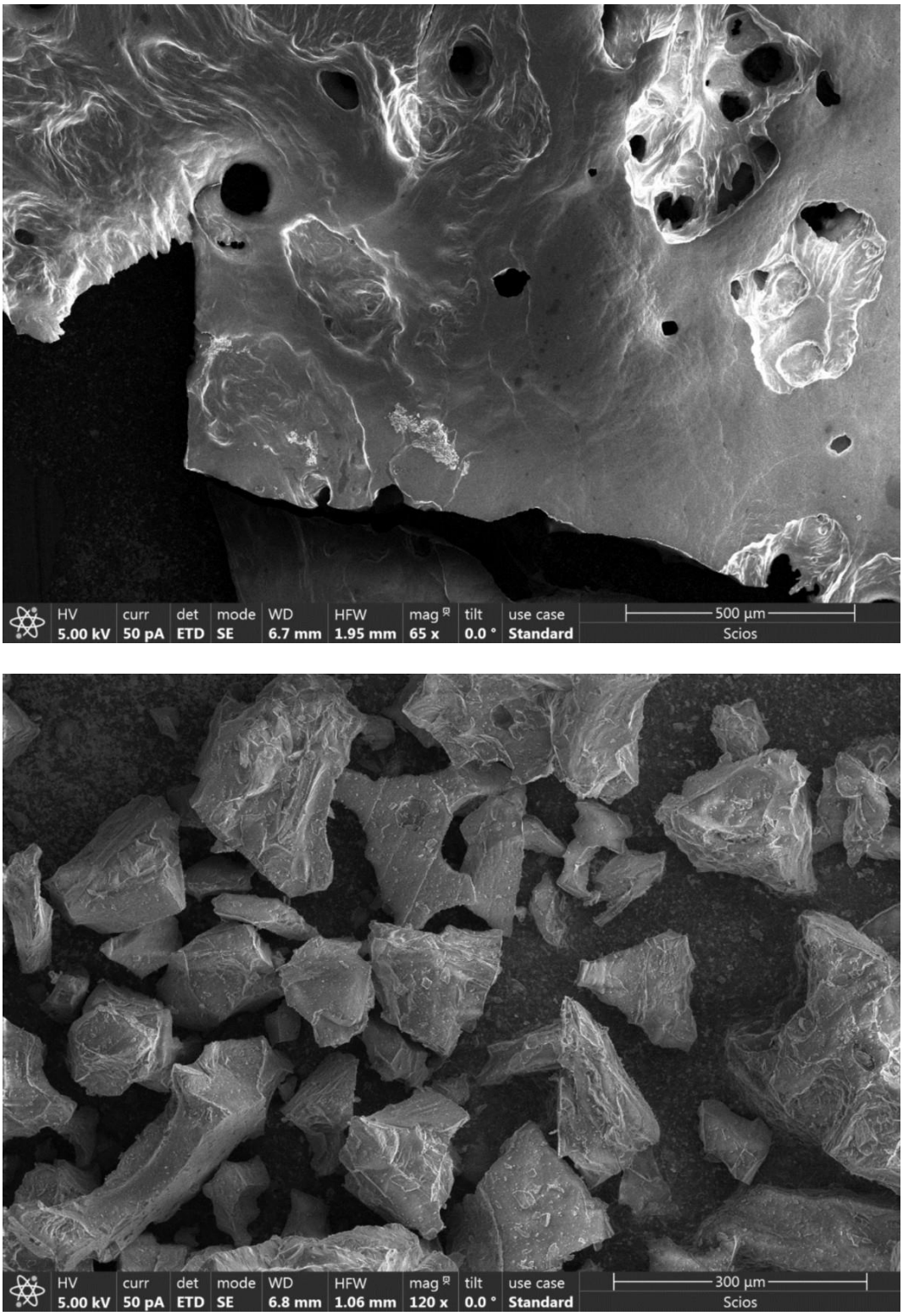

Figure S8. SEM images of sample **6_03** prior to calcination and grinding (top) and afterwards (bottom). For measurements, a Scios Dual Beam from FEI (5 kV/50 pA) was used.

4.2 Lattice parameter

For lattice parameters larger than approximately 25 nm, the values could not be determined from SAXS measurements anymore, because the required ultra-small angle regime was not accessible with the available measurement device. To give an idea about the dimension of the lattice parameters of OMS (ordered mesoporous silica) materials prepared from very large polyethers, the values were estimated from TEM images for two representative samples (Figure S8).

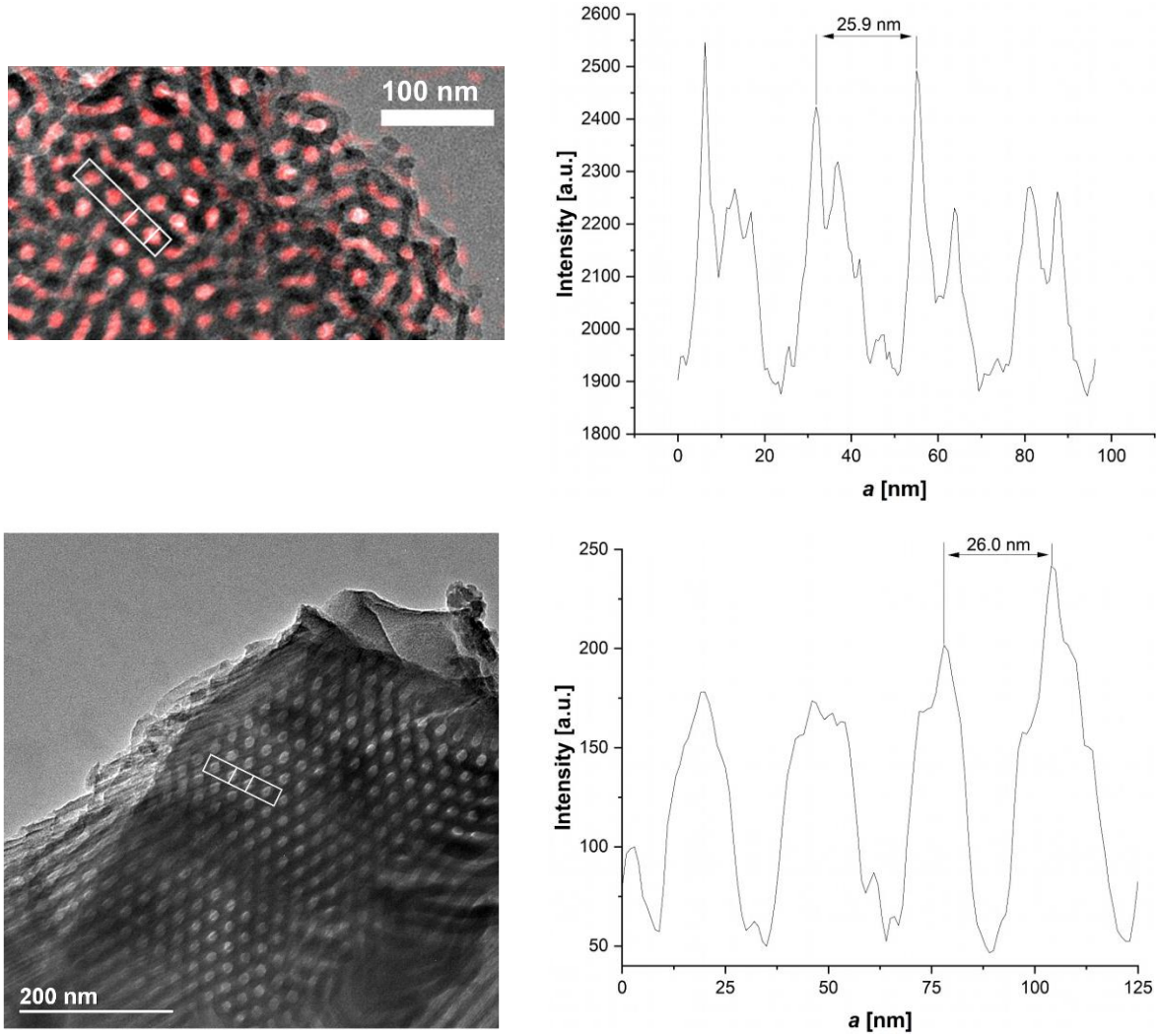

Figure S9. TEM image analysis of sample **20-b^{RT}** (top) and **8-e^{RT}** (bottom). The white rectangles indicate the micrograph areas, which were used to plot the intensity profiles to the right. The distance between the maxima of the intensity profiles approximates the lattice parameter *a* of the respective sample.

4.3 Small angle X-ray scattering (SAXS)

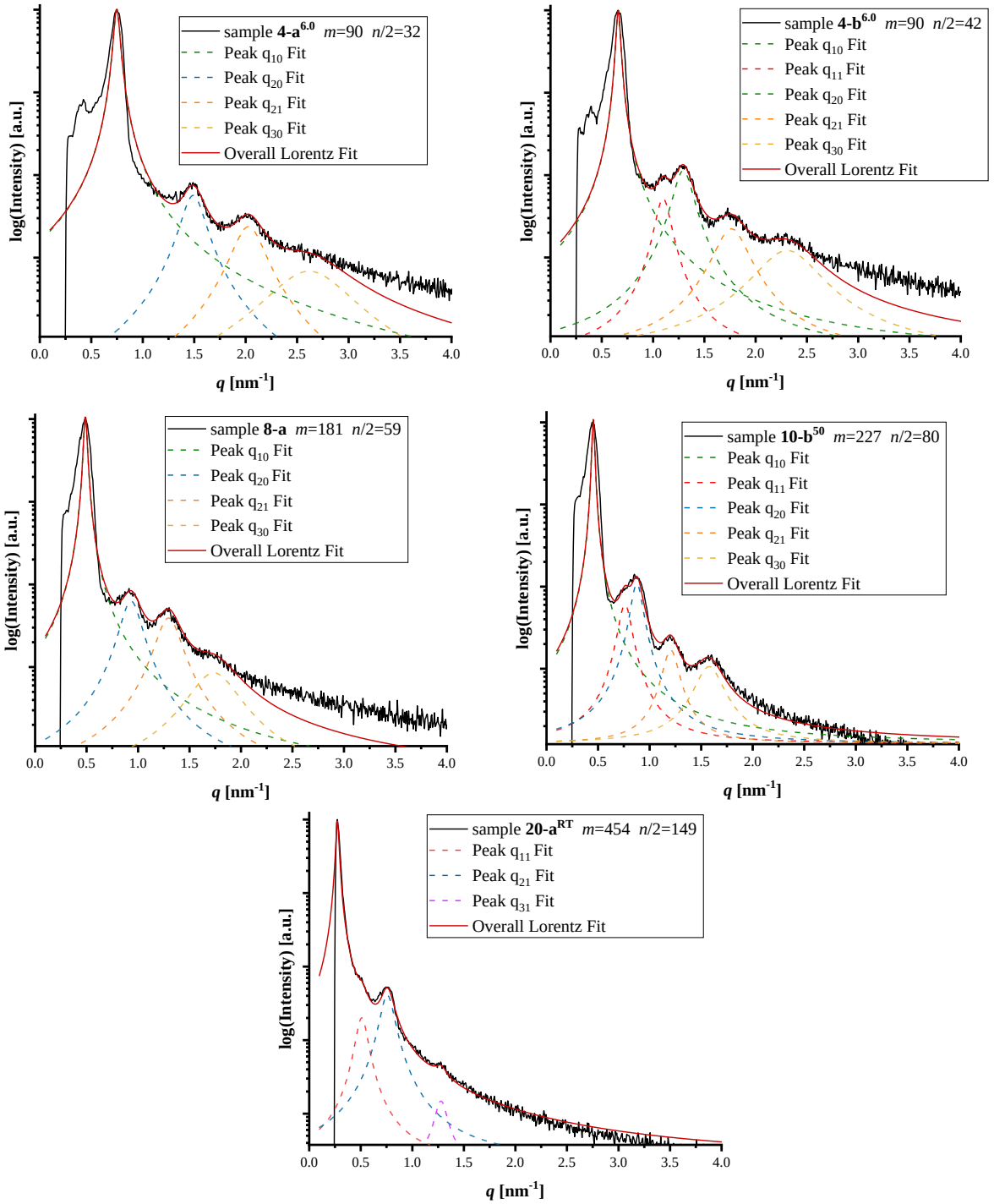

Figure S10. Representative examples for SAXS analysis of OMS samples derived from PEO 4000, 8000, 10 000 and 20 000 polyether templates. The scattering maxima were extracted by fitting them to Lorentz distributions. For each peak the Miller Indices (*hk*) were assigned, confirming the 2D hexagonal symmetry of the OMS materials. For the OMS prepared with largest polyether (m = 454, $n/2$ = 149) the (10)-peak is cut off by the beam stop at low q-values. Nonetheless, it is possible to identify the hexagonal structure of the material due to the three further scattering maxima.

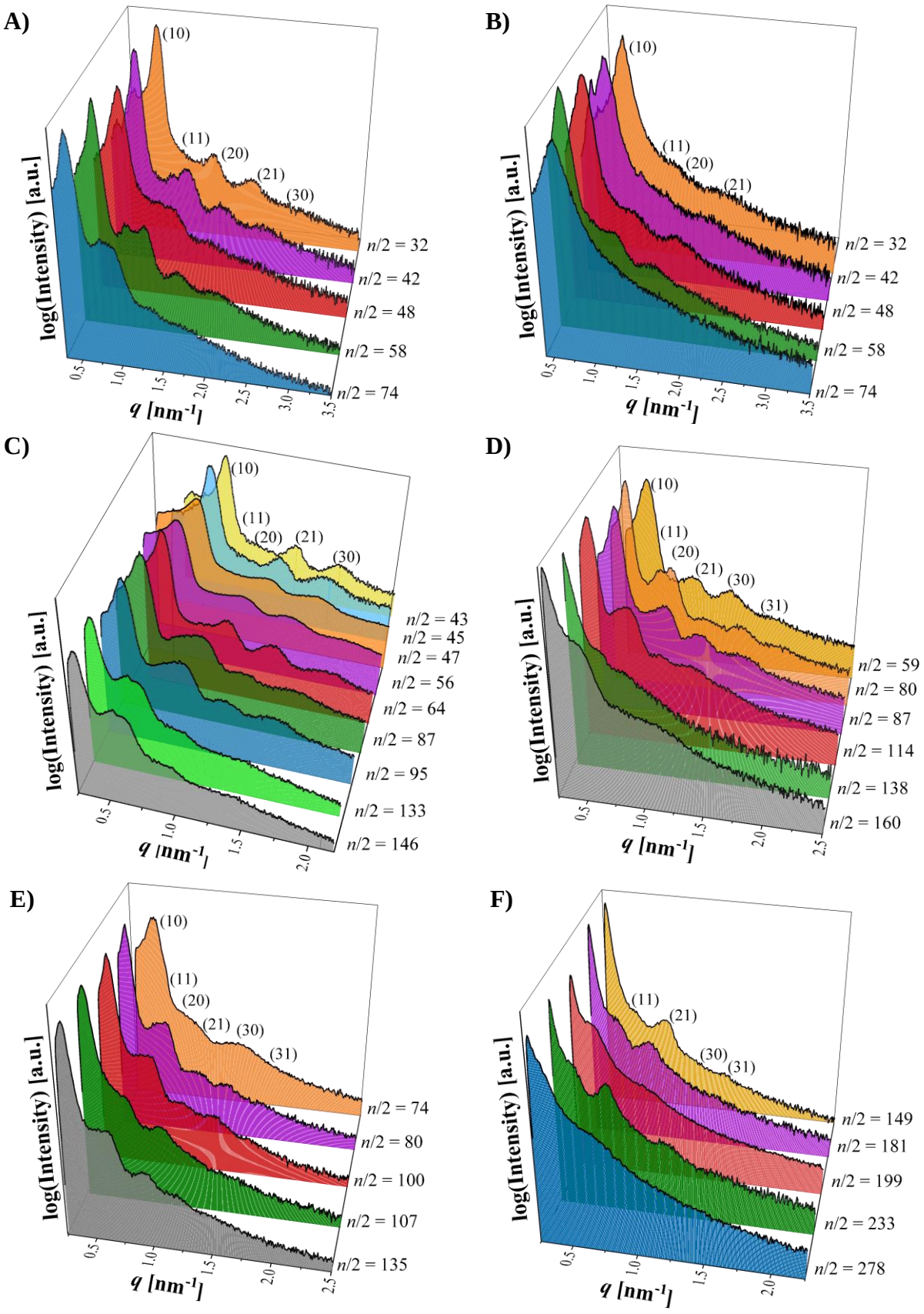

Figure S11. SAXS analysis of OMS samples derived from **A)** PEO 4000 (n(H2O)/n(TMOS) = 6.0), **B)** PEO 4000 (n(H2O)/n(TMOS) = 4.0), **C)** PEO 6000, **D)** PEO 8000, **E)** PEO 10 000 and **F)** PEO 20 000 polyether templates. The Miller Indices (hk) were assigned, confirming the 2D hexagonal symmetry of the OMS materials.

4.4 N_2-sorption measurements

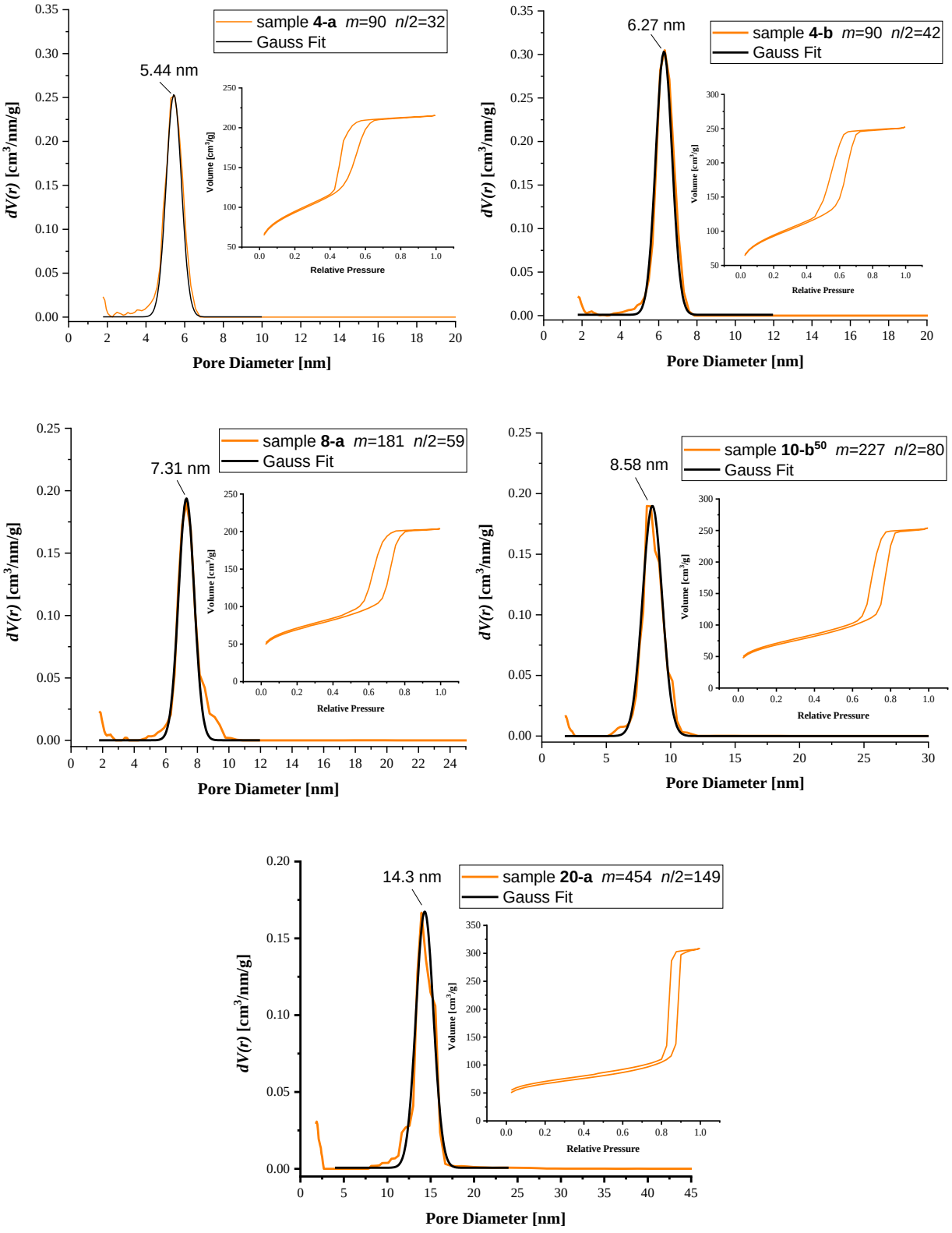

Figure S12. Representative examples for N_2-sorption diagrams of OMS samples derived from PEO 4000, 8000, 10 000 and 20 000 polyether templates. The maxima of the pore-size distribution were determined by Gauss Fits. Additionally the isotherms of the samples are displayed.

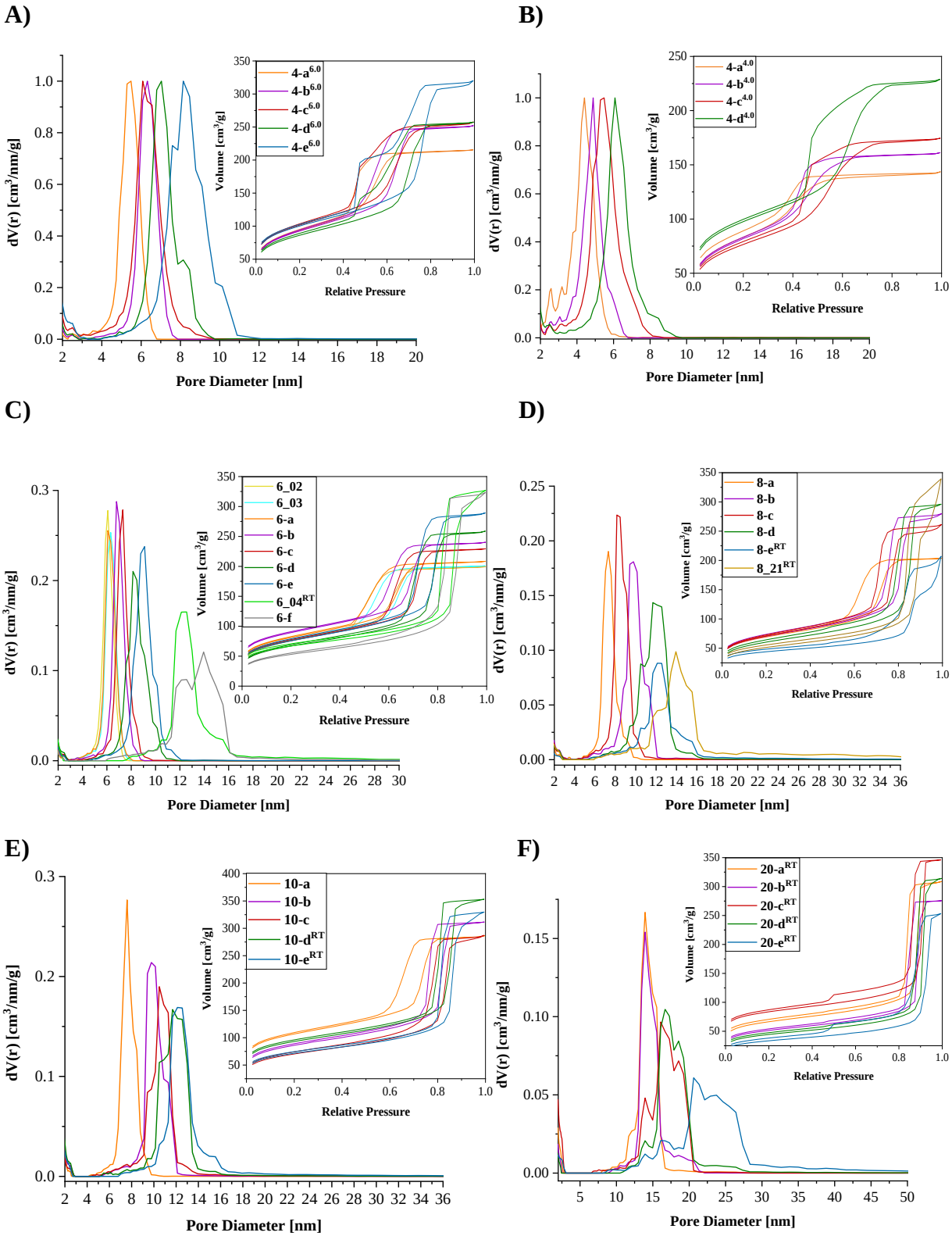

Figure S13. N_2-sorption diagrams and isotherms of OMS samples derived from **A)** PEO 4000 (*n*(H2O)/*n*(TMOS) = 6.0), **B)** PEO 4000 (*n*(H2O)/*n*(TMOS) = 4.0), **C)** PEO 6000, **D)** PEO 8000, **E)** PEO 10 000 and **F)** PEO 20 000 polyether templates.

4.5 Investigation of the molar ratio $n(H_2O)/n(TMOS) = 4.0$

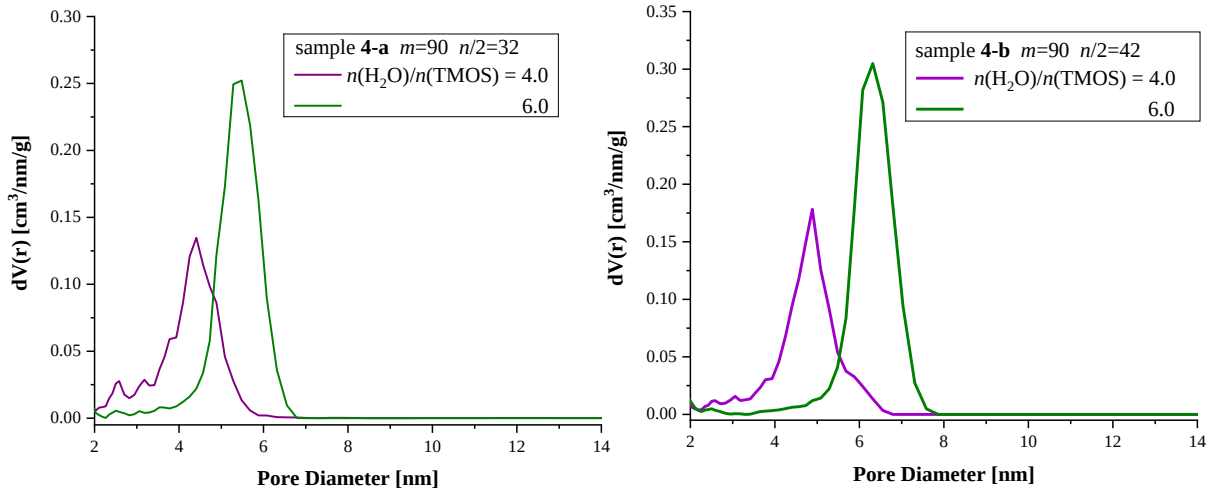

Figure S14. Representative N_2-sorption diagrams of OMS samples derived from PEO 4000 using $n(H_2O)/n(TMOS) = 6.0$ (marked in green) in comparison with the samples using $n(H_2O)/n(TMOS) = 4.0$ (marked in purple).

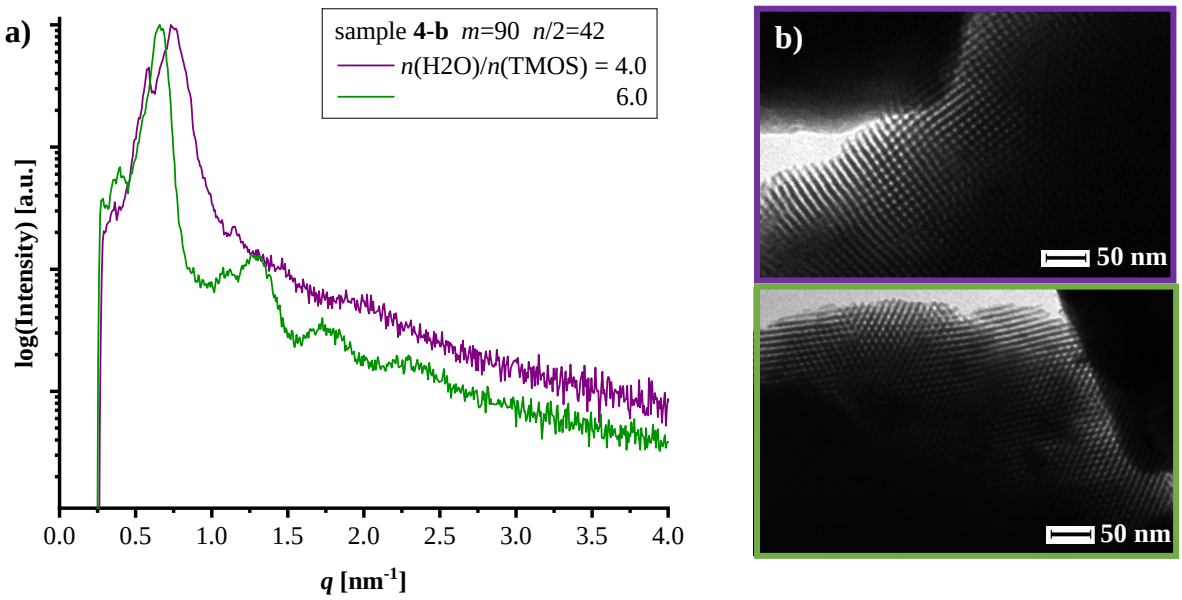

Figure S15. a) SAXS analysis of OMS sample **4-b** derived from PEO 4000 using $n(H_2O)/n(TMOS) = 6.0$ (marked in green) and $n(H_2O)/n(TMOS) = 4.0$ (marked in purple). b) Additionally, the transmission electron micrographs of the calcined OMS are displayed.

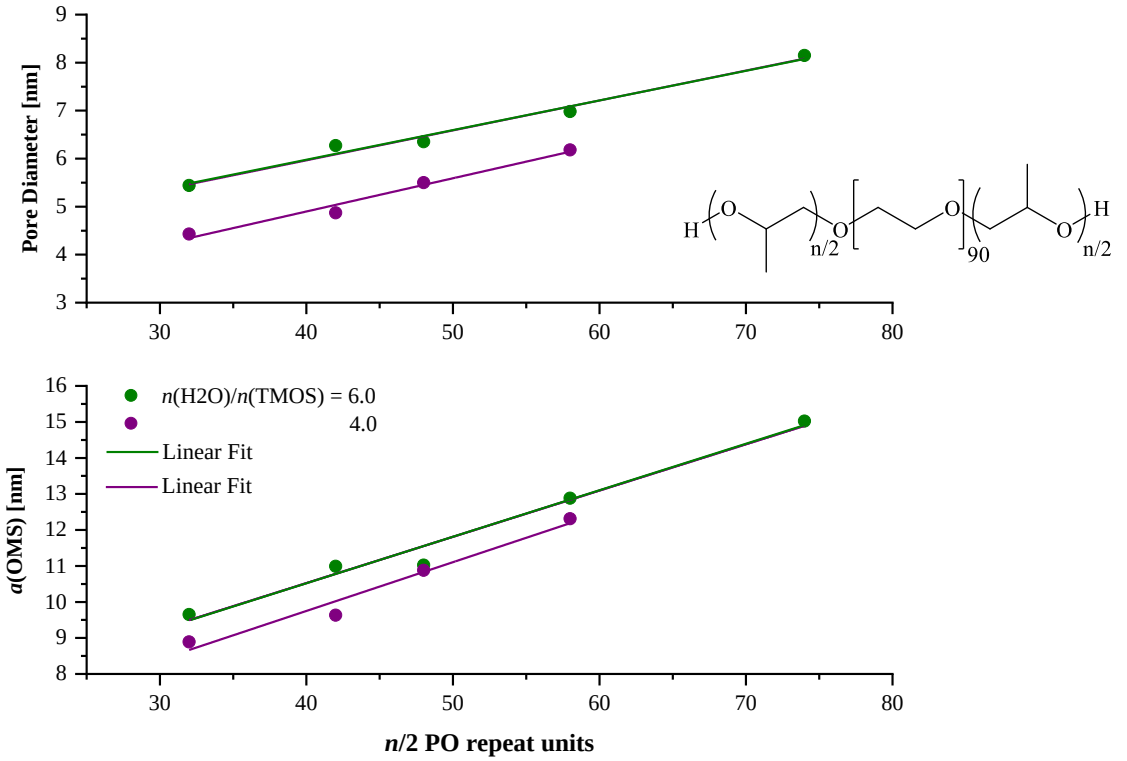

Figure S16. Cell parameter *a* and pore diameter are plotted versus the *n*/2 PO repeat units for OMS samples derived from PEO 4000 using $n(H_2O)/n(TMOS)$ = 6.0 (marked in green) and $n(H_2O)/n(TMOS)$ = 4.0 (marked in purple).

4.6 Ultra-large mesopores

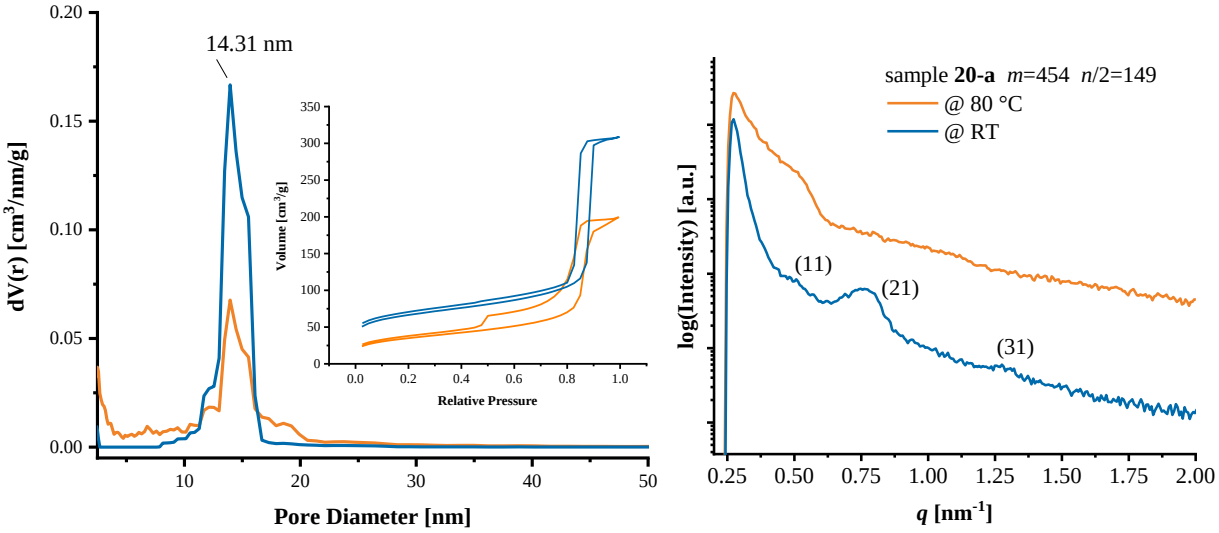

Figure S17. Comparison of N_2-sorption diagrams and isotherms of OMS sample **20-a** derived from high molecular weight PEO 20 000 polyether template by using different temperatures during hydrothermal treatment: @RT (room temperature, marked in blue), @80 °C (marked in orange). Additionally the SAXS patterns are shown. For each peak the Miller Indices (*hk*) were assigned, confirming the 2D hexagonal symmetry of the OMS materials. The (10)-peak is cut off by the beam stop at low *q*-values.

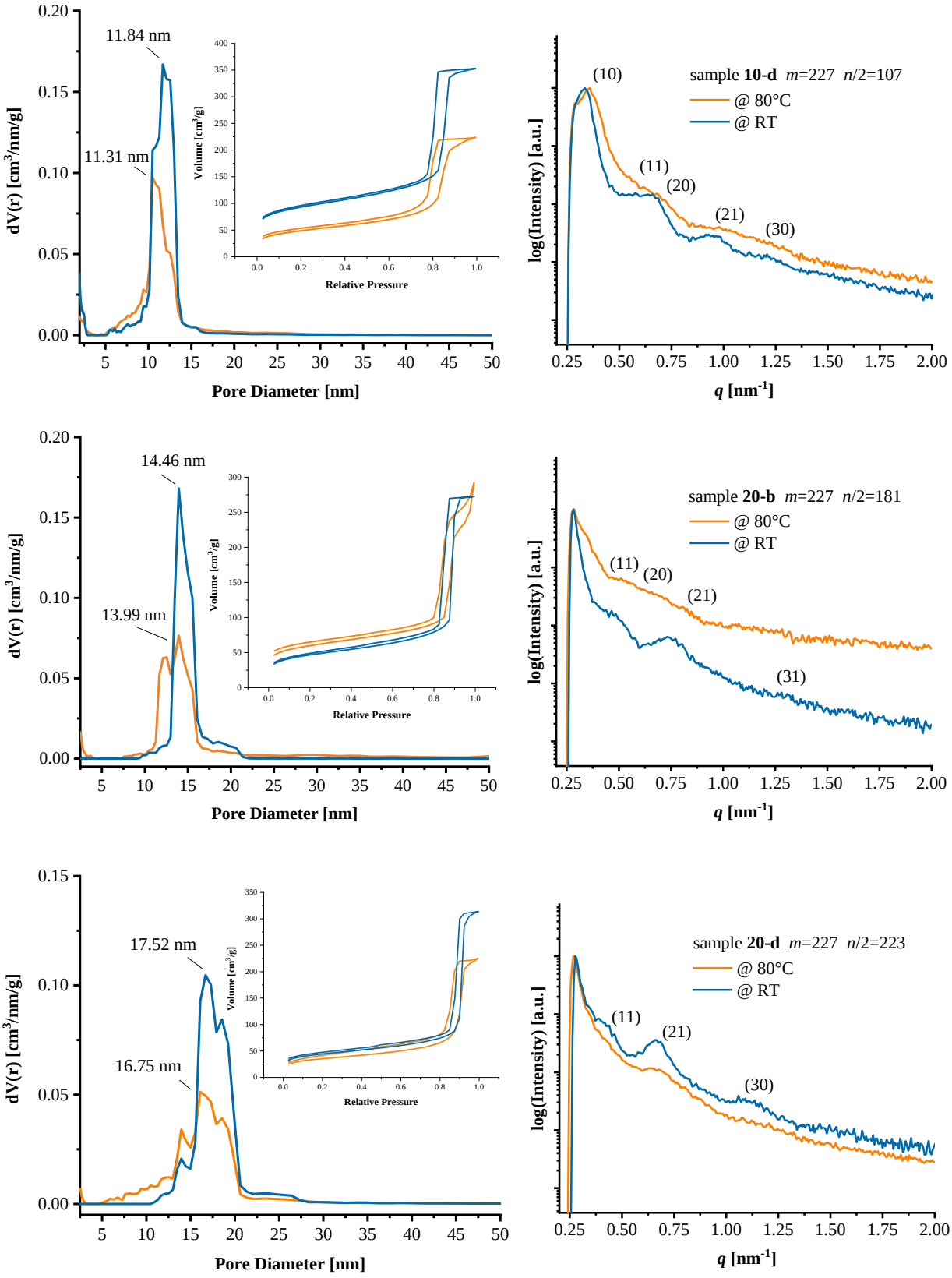

Figure S18. Comparison of N_2-sorption diagrams of more representative OMS samples derived from PEO 10 000 and 20 000 polyether templates (n/2 PO > 100) by using different temperatures during hydrothermal treatment.

4.7 Correlation of PO repeat units (*n*/2) with the pore diameter

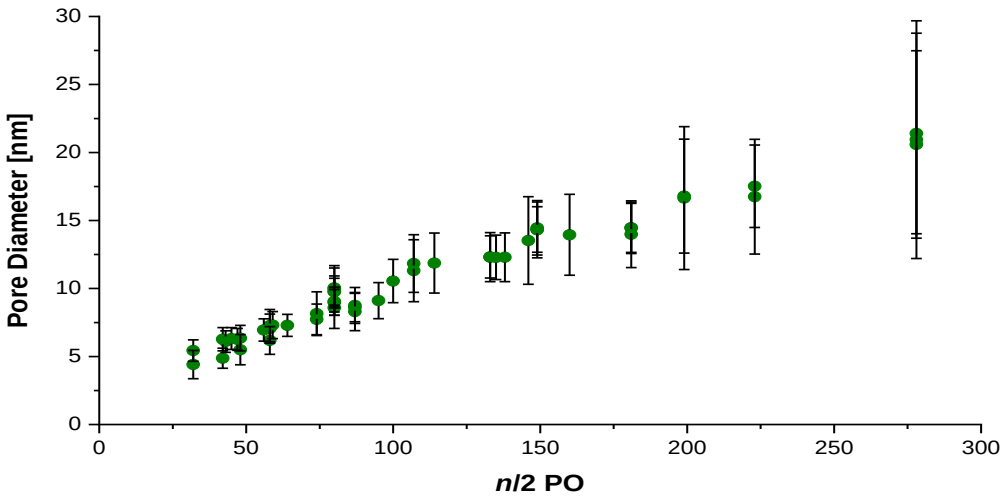

Figure S19. Correlation of PO repeat units (*n*/2) of the polyether template with corresponding OMS pore diameters. The maxima of the pore-size distribution were determined by Gauss Fits and the error bars represent the standard deviation of the peak maximum.

4.8 Reproducibility

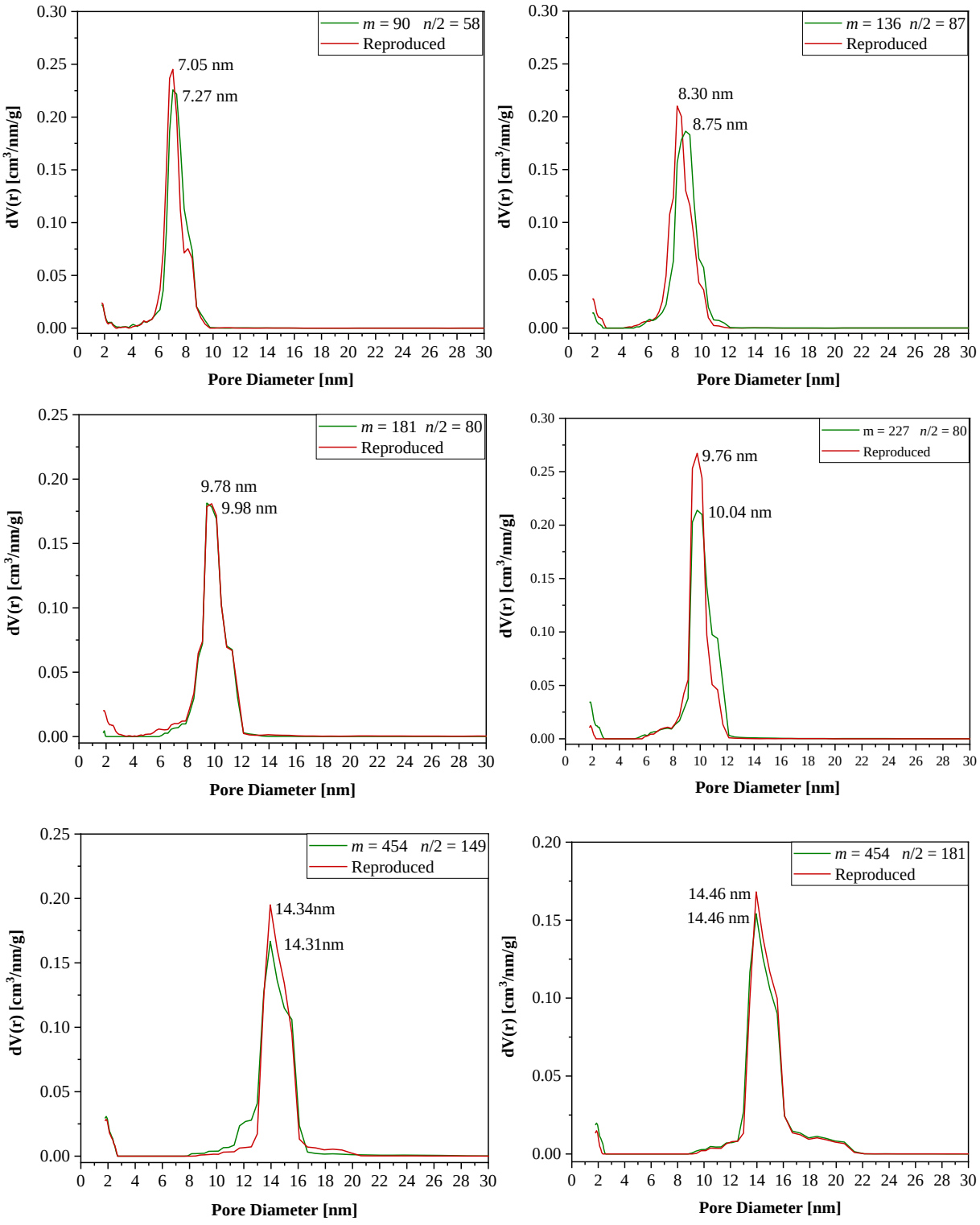

Figure S20. Several examples of OMS samples derived from PEO 4000, 6000, 8000, 10 000 and 20 000 polyether templates and corresponding repeat experiments.

5 Tabular data

Table S1 Characterization parameters of all employed block copolyethers ($PPO_{n/2}$-EO_m-$PPO_{n/2}$) and the properties of the resulting silica materials. (no data = no ordered mesoporous silica received, n.d. = non-determinable or not determined, bold = data from Table **1** in the manuscript).

sample	PEO [*m*]	PPO [a)] [*n*/2]	HLB	M_n (calc.)[a)] [g mol^{-1}]	$Đ_M$ [b)]	$n_{(H2O)}/n_{(TMOS)}$	H_α [wt%]	d_{pore} [c)] [nm]	a_{OSM} [d)] [nm]	a_{LCC} [d)] [nm]	V_{total} [c)] [cm^3/g]	SSA_{total} [c)] [m^{2}g/]
4-a$^{6.0}$		**32**	**10.3**	**7 700**	**1.08**	**6.0**	**40**	**5.44**	**9.71**	**13.97**	**0.320**	**320.77**
4-a		32	10.3	7 700	1.08	4.0	40	4.41	8.89	13.97	0.211	286.50
4-b$^{6.0}$		**42**	**9.0**	**8 800**	**1.08**	**6.0**	**40**	**6.27**	**10.99**	**15.91**	**0.376**	**319.27**
4-b		42	9.0	8 800	1.08	4.0	40	4.87	9.63	15.91	0.238	280.05
4-c$^{6.0}$		**48**	**8.4**	**9 500**	**1.10**	**6.0**	**40**	**6.35**	**11.02**	**18.18**	**0.383**	**363.22**
4-c	90	48	8.4	9 500	1.10	4.0	40	5.50	10.88	18.18	0.259	266.00
4-d$^{6.0}$	(PEO 4000)	**58**	**7.4**	**10 700**	**1.08**	**6.0**	**40**	**7.05**	**12.88**	**19.29**	**0.385**	**306.36**
4-d$^{6.0*}$		58	7.4	10 700	1.08	6.0	40	7.27	13.08	19.29	0.385	295.70
4-d		58	7.4	10 700	1.08	4.0	40	6.18	12.31	19.29	0.340	361.70
4-e$^{6.0}$		**74**	**6.3**	**12 600**	**1.06**	**6.0**	**40**	**8.15**	**15.02**	**24.34**	**0.478**	**368.32**
4-e		74	6.3	12 600	1.06	4.0	40	-	-	-	-	-
6_01		39	11.3	10 600	1.08	4.0	-	-	-	-	-	-
6_02		43	11.0	10 900	1.08	4.0	50	6.10	11.30	n.d.	0.297	255.56
6_03		45	10.7	11 200	1.07	4.0	50	6.32	11.97	n.d.	0.300	265.35
6-a		**47**	**10.4**	**11 500**	**1.07**	**4.0**	**50**	**6.26**	**12.17**	**19.09**	**0.311**	**287.58**
6-b		**56**	**9.6**	**12 600**	**1.08**	**4.0**	**50**	**6.95**	**13.36**	**18.99**	**0.359**	**329.69**
6-c		**64**	**8.9**	**13 500**	**1.08**	**4.0**	**50**	**7.29**	**13.77**	**20.32**	**0.344**	**266.69**
6-d	136	**87**	**7.4**	**16 100**	**1.07**	**4.0**	**50**	**8.30**	**15.44**	**21.34**	**0.408**	**300.05**
6-d*	(PEO 6000)	87	7.4	16 100	1.07	4.0	50	8.75	16.16	21.34	0.389	233.20
6-e		**95**	**7.1**	**16 900**	**1.06**	**4.0**	**50**	**9.11**	**16.41**	**n.d.**	**0.435**	**267.24**
6_04		133	5.6	21 400	1.06	4.0	50	12.31	21.28	n.d.	0.566	216.85
6_04^{RT}		133	5.6	21 400	1.06	4.0	50	12.32	21.43	n.d.	0.493	254.38
6-f		**146**	**5.2**	**22 900**	**1.06**	**4.0**	**50**	**13.53**	**21.95**	**n.d.**	**0.487**	**184.43**
6_05^{RT}		155	5.0	24 000	1.07	4.0	50	-	-	-	-	-

[a)] Determined via ^{1}H NMR, [b)] determined from GPC ($CHCl_3$), [c)] pore diameter (d_p), total pore volume (V_{total}) and total specific surface area (SSA_{total}) determined via N_2 sorption (DFT (density functional theory) method), [d)] hexagonal lattice parameter (a) determined via SAXS analysis, *reproduced, ^{RT} hydrothermal treatment at room temperature, $^{6.0}$ $n_{(H2O)}/n_{(TMOS)}$ = 6.0

sample	PEO [*m*]	PPO [a] [*n*/2]	HLB	M_n (calc.) [a] [g mol^{-1}]	$Đ_M$ [b]	$n_{(H2O)}/n_{(TMOS)}$	H_α [wt%]	d_{pore} [c] [nm]	a_{OSM} [d] [nm]	a_{LCC} [d] [nm]	V_{total} [c] [cm^3/g]	SSA_{total} [c] [m^{2}g/]
8-a		**59**	**10.7**	**14 800**	**1.06**	**4.0**	**50**	**7.31**	**14.87**	**23.63**	**0.306**	**253.23**
8-b[55]		80	9.3	17 200	1.03	4.0	55	9.05	16.84	n.d.	0.381	245.82
8-b		**80**	**9.3**	**17 200**	**1.03**	**4.0**	**60**	**9.78**	**17.48**	**27.17**	**0.420**	**252.08**
8-b*	181	80	9.3	17 200	1.03	4.0	60	9.98	18.80	27.17	0.367	175.44
8-c	(PEO 8000)	**87**	**8.8**	**18 000**	**1.02**	**4.0**	**60**	**8.60**	**16.23**	**26.97**	**0.389**	**248.01**
8-d		**114**	**7.5**	**21 200**	**1.03**	**4.0**	**55**	**11.87**	**20.60**	**28.34**	**0.448**	**211.89**
8-e^{RT}		**138**	**6.6**	**24 000**	**1.02**	**4.0**	**60**	**12.30**	**n.d.**	**n.d.**	**0.300**	**120.03**
8-f^{RT}		**160**	**6.0**	**26 500**	**-**	**4.0**	**60**	**13.95**	**24.18**	**n.d.**	**0.491**	**185.61**
10-a		**74**	**10.9**	**18 300**	**1.07**	**4.0**	**50**	**7.73**	**15.46**	**n.d.**	**0.429**	**423.92**
10-b[50]		80	10.4	19 300	1.07	4.0	50	8.58	15.98	23.56	0.382	240.60
10-b[55]		80	10.4	19 300	1.07	4.0	55	8.98	14.66	n.d.	0.367	306.83
10-b		**80**	**10.4**	**19 300**	**1.07**	**4.0**	**60**	**10.04**	**18.37**	**23.56**	**0.470**	**325.81**
10-b*	227	80	10.4	19 300	1.07	4.0	60	9.76	18.18	23.56	0.417	214.87
10-c	(PEO 10 000)	**100**	**9.2**	**21 600**	**1.06**	**4.0**	**60**	**10.55**	**20.21**	**26.97**	**0.432**	**259.27**
10-d		107	8.9	22 500	1.07	4.0	60	11.31	20.32	26.67	0.338	170.37
10-d^{RT}		**107**	**8.9**	**22 500**	**1.07**	**4.0**	**60**	**11.84**	**21.70**	**26.67**	**0.534**	**366.12**
10-e^{RT}		**135**	**7.8**	**25 600**	**1.07**	**4.0**	**60**	**12.29**	**21.78**	**n.d.**	**0.498**	**269.40**
20-a		149	10.7	37 300	1.10	4.0	60	14.46	n.d.	n.d.	0.454	536.63
20-a^{RT}		**149**	**10.7**	**37 300**	**1.10**	**4.0**	**60**	**14.31**	**n.d.**	**n.d.**	**0.468**	**257.20**
20-a^{RT*}		149	10.7	37 300	1.10	4.0	60	14.34	n.d.	n.d.	0.450	241.21
20-b		181	9.8	41 000	1.14	4.0	60	13.99	n.d.	n.d.	0.413	231.14
20-b^{RT}		**181**	**9.8**	**41 000**	**1.14**	**4.0**	**60**	**14.46**	**n.d.**	**n.d.**	**0.420**	**194.47**
20-b^{RT*}		181	9.8	41 000	1.14	4.0	60	14.46	n.d.	n.d.	0.415	173.02
20-c^{RT}	454	**199**	**9.3**	**43 100**	**1.06**	**4.0**	**60**	**16.79**	**n.d.**	**n.d.**	**0.526**	**338.66**
20-c^{RT*}	(PEO 20 000)	199	9.3	43 100	1.06	4.0	60	16.65	n.d.	n.d.	0.490	298.96
20-d		223	8.5	47 000	1.14	4.0	60	16.75	n.d.	n.d.	0.340	124.39
20-d^{RT}		**223**	**8.5**	**47 000**	**1.14**	**4.0**	**60**	**17.52**	**n.d.**	**n.d.**	**0.479**	**161.22**
20-e		278	7.6	52 300	1.25	4.0	60	20.94	n.d.	n.d.	0.334	86.17
20-e^{RT}		278	7.6	52 300	1.25	4.0	60	21.40	n.d.	n.d.	0.547	150.25
20-e^{RT*}		**278**	**7.6**	**52 300**	**1.25**	**4.0**	**60**	**20.59**	**n.d.**	**n.d.**	**0.385**	**118.17**

[a] Determined via ^{1}H NMR, [b] determined from GPC ($CHCl_3$), [c] pore diameter (d_p), total pore volume (V_{total}) and total specific surface area (SSA_{total}) determined via N_2 sorption (DFT (density functional theory) method), [d] hexagonal lattice parameter (a) determined via SAXS analysis, *reproduced, RT hydrothermal treatment at room temperature, $^{6.0}$ $n_{(H2O)}/n_{(TMOS)}$ = 6.0

6 Microporosity

Considering that microporosity in OMS is thought to originate from the hydrophilic parts of the surfactants dangling into the solute,[4] the micropore volume (V_{micro}) should increase with increasing hydrophilic block size. For **4-b$^{6.0}$**, templated with PPO_{42}-PEO_{90}-PPO_{42}, a micropore volume of 0.036 cm^3/g was obtained, which is less than 10 % of the total pore volume. For OMS prepared by a standard liquid crystal templating process with commercial Pluronics possessing significantly shorter hydrophilic blocks (PEO_{19}-PPO_{69}-PEO_{19} or PEO_{17}-PPO_{58}-PEO_{17}), values of V_{micro} are typically two to three times larger.[5–7] For **20-a**, templated with PPO_{149}-PEO_{454}-PPO_{149}, a similar value of V_{micro} was found as for conventional materials, even though the hydrophilic block is significantly larger. A reduced microporosity was already reported for OMS prepared by the true liquid crystal templating process (V_{micro} = 0.07 cm^3/g) compared to a conventional liquid crystal templating process (V_{micro} = 0.12 cm^3/g).[8] The even lower value found for **4-b$^{6.0}$** in this study might additionally originate from the reverse structure of the polyethers, with the hydrophilic part of the polymer being located in the middle of the molecules. This prevents an extensive "dangling" of the hydrophilic moieties out of the micelles, as it is present for normal poloxamers. Of course, further data is needed to confirm this assumption.

Interestingly, the microporosity is reduced dramatically when the curing temperature is reduced from 80°C (V_{micro} = 0.136 cm^3/g) to room temperature (V_{micro} = 0.041 cm^3/g), for the same surfactant (PPO_{149}-PEO_{454}-PPO_{149}). This poses a strong contrast to OMS prepared by the conventional liquid crystal templating process, for which the microporosity is typically reduced for increasing synthesis temperatures.[4,9]

Table S2: Direct comparison of micro- and mesoporosity for representative silica materials.

sample	**Micropores + Mesopores** SSA_{total} [m^2/g] / V_{total} [cm^3/g][a)]	**Micropores** SSA_{Micro} [m^2/g] / V_{Micro} [cm^3/g][a)]
4-b$^{6.0}$	319 / 0.376	85 / 0.036
20-a	454 / 0.454	324 / 0.136
20-a^{RT*}	257 / 0.468	94 / 0.041

[a)] Determined *via* N_2-sorption.

7 Available raw data

Raw data, which was acquired for the preparation of the manuscript, was stored in the data repository of the University of Stuttgart (DaRUS) and is openly accessible via following link: https://doi.org/10.18419/darus-2374

The available raw data comprises:

- ^{1}H NMR spectra of all synthesized block copolymers
- GPC measurements of all synthesized block copolymers
- SAXS data of all synthesized OMS materials
- N_2-physisorption data (isotherms and DFT analysis) of all synthesized OMS materials

References

1 S. Naumann, A. W. Thomas and A. P. Dove, *ACS Macro Lett.*, 2016, **5**, 134.
2 N. Kuhn, H. Bohnen, J. Kreutzberg, D. Bläser and R. Boese, *J. Chem. Soc., Chem. Commun.*, 1993, 1136.
3 R. F. T. Stepto, *Pure and Applied Chemistry*, 2009, **81**, 351.
4 A. Galarneau, H. Cambon, F. Di Renzo, R. Ryoo, M. Choi and F. Fajula, *New J. Chem.*, 2003, **27**, 73.
5 V. Meynen, P. Cool and E. F. Vansant, *Microporous Mesoporous Mater.*, 2009, **125**, 170.
6 P. Martinot-Lagarde, *J. Phys. Colloques*, 1976, **37**, C3-129-C3-132.
7 K. Miyazawa and S. Inagaki, *Chem. Commun.*, 2000, **21**, 2121.
8 S. G. Wainwright, C. M. Parlett, R. A. Blackley, W. Zhou, A. F. Lee, K. Wilson and D. W. Bruce, *Microporous Mesoporous Mater.*, 2013, **172**, 112.
9 A. Galarneau, H. Cambon, F. Di Renzo and F. Fajula, *Langmuir*, 17, **2001**, 8328.